Electron Transfer in Dinuclear Cobalt Complexes with "Non-Innocent" Bridging Ligands**

Katja Heinze, Gottfried Huttner,* Laszlo Zsolnai, Albrecht Jacobi and Peter Schober

Abstract: Reaction of tripod cobalt(II) templates $[\{CH_3C(CH_2PAr_2)_3\}Co^{II}]$ with potentially bridging ligands L generates the dinuclear compounds [(tripod)-Co-L-Co(tripod)]$^{2+}$. With L = oxalate ($C_2O_4^{2-}$) a biscobalt(II) complex (**1**) is formed, while with L = $C_6H_2O_4^{2-}$, the dianion derived from 2,5-dihydroxy-1,4-benzoquinone (anilic acid), two-electron transfer within the dimetallic unit occurs and a biscobalt(III) charge distribution results (**2a**), as shown by X-ray structural analyses of **1** and **2a**, NMR spectroscopy, and theoretical investigations by the INDO method. Complex **2a** exhibits an unusually intense, low-energy absorption in its electronic spectrum; this is explained with a simple MO model. One-electron reduction of **2a** generates the corresponding mixed-valence complex, which is highly stabilised through extensive electron delocalisation. Substituents at the 3,6 positions of the bridging ligand (Cl, Br, I, NO_2, Me, *i*Pr, Ph; **2b**–**h**) as well as alkyl substitution at the aromatic rings of the tripod ligands (**3**, **4**) influence the optical and electrochemical properties consistent with the proposed model of charge distribution. Formal replacement of one $[(tripod)Co^{III}]^{3+}$ moiety by $[CH_2]^{2+}$ leads to the mononuclear complex **6**, which is shown to be a typical [(tripod)Co^{III}-(catecholato)]$^+$ complex. Therefore the substantially different optical and electrochemical properties of the dinuclear complexes with respect to those of **6** result from strong metal–metal interactions mediated by the bridging ligand.

Keywords
bridging ligands · charge transfer · cobalt · quinones · tripodal ligands

Introduction

Complexes that combine "non-innocent" ligands, especially dioxolene ligands (diox), with transition-metal ions that have two or more accessible oxidation states give rise to questions concerning the charge distribution and effective oxidation states in these compounds.[1] In their complexes dioxolene ligands can be found in three different formal oxidation states (Figure 1): neutral quinones (q), radical semiquinones (sq), and dianionic catecholates (cat). The small energy gap between dioxolene π^* orbitals and metal d_π orbitals results in significant sensitivity of the charge distribution within the metal complexes towards the molecular environment.

Coordination of one dioxolene ligand to a metal centre M results in the formation of compounds of type **A** (Figure 1). For example the species [(L-L)Cu(diox)] (with L–L = 2,2′-bipyridine (bpy)) is best described as [(bpy)Cu^{II}(cat)],[2] while substitution of the hard nitrogen donor ligand 2,2′-bipyridine with the soft phosphane donor ligand PPh_3 results in the [$(PPh_3)_2Cu^{I}$(sq)] charge distribution.[3] With ruthenium as the central metal [$(bpy)_2Ru^{II}$(sq)]$^+$ complexes can be obtained which have a considerable admixture of the [$(bpy)_2Ru^{III}$(cat)]$^+$ electronic configuration.[4] In [(tripod)Co(diox)]$^+$ complexes electron delocalisation seems to be small, resulting in a relatively pure Co^{III}–cat ground state.[5]

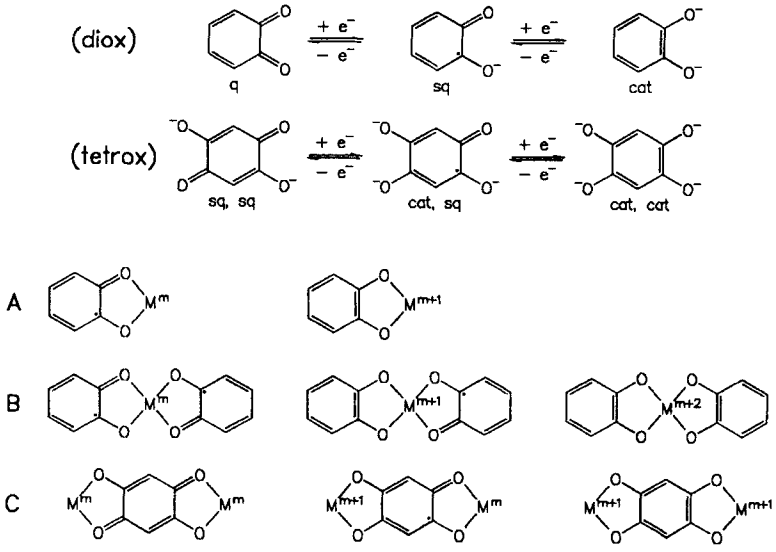

Figure 1. Coordination modes of dioxolene ligands.

[*] Prof. Dr. G. Huttner, K. Heinze, L. Zsolnai, A. Jacobi, P. Schober
Anorganisch-Chemisches Institut, Universität Heidelberg
Im Neuenheimer Feld 270, D-69120 Heidelberg (Germany)
Fax: Int. code +(6221)54-5707
e-mail: katja@sun0.urz.uni-heidelberg.de

[**] Part of this work was presented at the 31st International Conference on Coordination Chemistry, Vancouver (Canada), August **1996**.

0947-6539/97/0305-0732 $ 17.50+.50/0

Placing two "non-innocent" ligands on a redox-active metal centre (Figure 1, type **B**) leads to further possible electronic configurations. Ruthenium complexes of this type again show relatively large charge delocalisation in $[(bpy)Ru(diox)_2]^-$ and $[(bpy)Ru(diox)_2]$ complexes.[6] Thermal equilibria instead of quantum-mechanical mixing have been found in complexes with cobalt[7] and manganese[8] metal centres. These valence tautomeric equilibria can be observed in solution as well as in the solid state, and they depend considerably on the nature of the counterligand[7e–7g] and the solid-state structures (e.g., solvate molecules)[7b]. The equilibrium concentration of the valence isomers can be influenced by applying an external perturbation (temperature,[7a–7g, 8] pressure,[7h] light[7i, 7j]).

Inverting the composition ratio of the type **B** species [(diox)–M–(diox)] corresponds to the dinuclear compounds [M–(tetrox)–M] (Figure 1, type **C**). The "non-innocent" bridging ligand tetrox, derived from the dianion of 2,5-dihydroxy-1,4-benzoquinone, can in principle bind to metal ions in three different oxidation states (Figure 1): as a dianion (sq, sq), as a radical trianion (cat, sq), and as a tetraanion (cat, cat). Dinuclear complexes of this type with paramagnetic metal ions [Cu^{II},[9] Ni^{II},[10] Fe^{III}[11]] have been prepared and investigated in order to study magnetic exchange interactions of two metal centres over a large distance. These complexes appear to have a rather localised charge distribution with the bridging ligand in the dianionic state (sq, sq). The same charge located on the bridging ligand is found in the [(cod)Rh^{I}(sq, sq)Rh^{I}(cod)] complex.[12] With the redox-active ruthenium metal centres this description does not seem to be appropriate because of substantial mixing between the metal d_π and ligand π^* orbitals.[13] In dinuclear complexes neither a charge distribution of the (cat, cat) type nor a bistable system analogous to the type **B** cobalt and manganese complexes has yet been observed.

We describe the synthesis and characterisation of a series of dinuclear metal complexes of type **C** (Figure 1) with cobalt ions as the redox active metal centres. As counterligands in these compounds tripodal phosphane ligands (1,1,1-tris(diphenylphosphanomethyl)ethane ($CH_3C(CH_2PPh_2)_3$), 1,1,1-tris(di-(*p*-tolyl)phosphanomethyl)ethane ($CH_3C(CH_2P(p\text{-tolyl})_2)_3$) and 1,1,1-tris(di-(*m*-xylyl)phosphanomethyl)ethane ($CH_3C(CH_2P(m\text{-xylyl})_2)_3$) are employed, which have been shown to stabilise cobalt in different oxidation states (+I, +II, +III).[5, 14, 15] This type of ligand coordinates facially to the metal ion because of its rigid backbone. The phosphane donor set induces a large ligand field splitting, which forces a coordination number of five for the cobalt ion (in the +II and +III oxidation states) and a low-spin configuration in the +II (d^7) and of course in the +III (d^6) oxidation states. The description of the ground and excited states of these new complexes will be derived by comparison with a formally analogous dinuclear tripod cobalt complex with a non-redox active bridging ligand (dianion of oxalic acid) and a mononuclear type **A** (Figure 1) $[(tripod)Co(diox)]^+$ complex. The influence of substituents (H, Cl, Br, I, NO_2, Me, *i*Pr, Ph) in the 3- and 6-positions of the bridging tetrox ligand as well as the effects of alkyl substituents at the aromatic rings of the tripod ligand will be discussed.

Results and Discussion

Syntheses of the complexes: The synthetic routes for the preparation of the dinuclear complexes **1**, **2a–h**, **3**, **4**, **5a** and **5b** and the mononuclear complexes **6** and **7** are presented in Figure 2. For the tetrafluoroborate salts **1**, **2a–h**, **3**, **4** and **6** the well-established reaction of the tripod ligand with the hexaaqua salt of $Co(BF_4)_2$ and subsequent addition of the coligand[16] results in the formation of the cationic tripod cobalt complexes. To obtain the hexafluorophosphate salts **5a,b** and **7** an alternative reaction procedure starting from $CoCl_2$ via the di(μ-chloro)-bis[(tripod)Co^{II}]$^{2+}$ complex[14b] has been established (Figure 2).

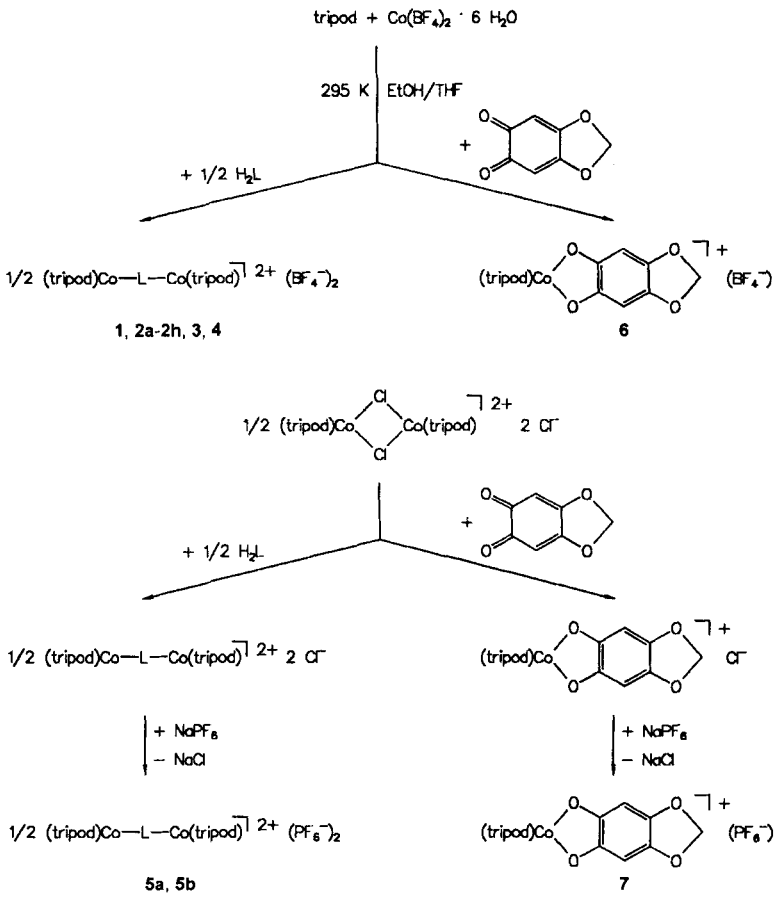

	L	tripod	counter ion
1	C_2O_4	$CH_3C(CH_2PPh_2)_3$	BF_4^-
2a-2h	$C_6O_4X_2$	$CH_3C(CH_2PPh_2)_3$	BF_4^-
	X =	H (2a), Cl (2b), Br (2c), I (2d), NO_2 (2e), Me (2f), *i*Pr (2g), Ph (2h)	
3	$C_6O_4H_2$	$CH_3C(CH_2P(p\text{-tolyl})_2)_3$	BF_4^-
4	$C_6O_4Cl_2$	$CH_3C(CH_2P(m\text{-xylyl})_2)_3$	BF_4^-
5a	$C_6O_4H_2$	$CH_3C(CH_2PPh_2)_3$	PF_6^-
5b	$C_6O_4Cl_2$	$CH_3C(CH_2PPh_2)_3$	PF_6^-
6	$C_7O_4H_4$	$CH_3C(CH_2PPh_2)_3$	BF_4^-
7	$C_7O_4H_4$	$CH_3C(CH_2PPh_2)_3$	PF_6^-

Figure 2. Syntheses of the di- and mononuclear Co complexes.

Structure and properties of 1: The μ-oxalato bridged complex **1** is obtained as a microcrystalline, red-brown compound. The FAB mass spectrum (Table 4) and elemental analysis confirm its dinuclear structure. The cyclic voltammogram of the complex salt **1** shows a reversible reduction wave at -0.31 V (vs. SCE) and an irreversible reduction at -0.6 V. The oxidation at a potential of 0.7 V is electrochemically irreversible. Electrolysis at a controlled potential of -0.53 V confirms that one electron per salt unit **1** is consumed. The electrochemical behaviour of **1** is therefore in good agreement with the behaviour of mononuclear [(tripod)Co^{II}(L–L)] complexes (L–L = O,O chelate, e.g. acetate,[14b] formate[14c]). The electronic spectrum of **1** in methylene chloride has weak absorptions at 481 nm ($\varepsilon = 1180\,M^{-1}cm^{-1}$) and 919 nm ($\varepsilon = 120\,M^{-1}cm^{-1}$). The latter can be assigned to a ligand-field transition. This also resembles the properties of other mononuclear low-spin [(tripod)Co^{II}-(L–L)] complexes.[14b]

The result of the structural analysis is shown in Figure 3. Compound **1** crystallises in the triclinic, centrosymmetric space

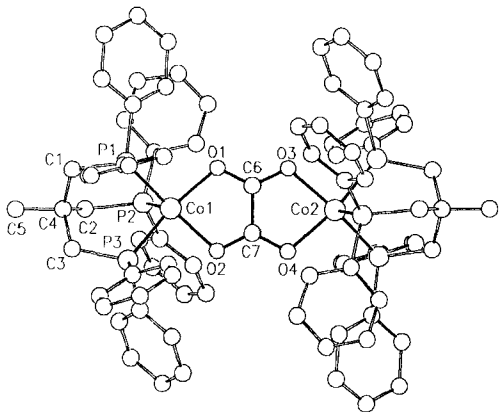

Figure 3. Perspective view of the dication of **1** [49].

group $P\bar{1}$. The centrosymmetric compound consists of discrete dinuclear dications and BF_4^- units. The dimeric cations are well separated from each other, the shortest intermolecular Co–Co distance being 1200 pm. Within the dimeric unit the metal centres are separated by 520 pm, which is a typical value for oxalato-bridged dimers.[17] The coordination polyhedron around the cobalt centre can be described as a distorted square pyramid with the P2 atom in the apical position. This apical Co–P2 bond is 7 pm longer than the basal ones (Table 1). The Co–O bond lengths (Table 1) fall within the range observed for comparable low-spin [(tripod)Co^{II}(L–L)] complexes.[14b,c] The C–O and C–C bond lengths (Table 1) of the planar oxalato ligand show no substantial deviation from those observed for other oxalato compounds.[17]

The EPR spectrum of **1** in methylene chloride at 295 K shows a broad unstructured signal centred at $g_{iso} \approx 2.11$. At 100 K in frozen methylene chloride the signal shows clearly the anisotropy of the g tensor, but individual g factors cannot be obtained, owing to the superposition of the signals. Two hyperfine splitting constants of 48 and 60 G (coupling to the ^{57}Co nucleus, $I = {}^7/_2$) can be extracted from the low- and high-field portions of the signal, respectively. These observations are in good agreement with those from previously described low-spin cobalt(II) complexes with the tripodal phosphine ligand.[15]

Table 1. Selected bond lengths (pm) [a] and angles (°) [a] [49].

	1	**2a**	**2b**	**2c**	**6**
Co1–O1	197.0(3)	189.8(5)	187.3(3)	186.3(6)	190.6(3)
Co1–O2	198.4(3)	188.3(5)	188.1(3)	186.3(6)	187.9(3)
C12–O3	–	–	–	–	136.5(4)
C12–O4	–	–	–	–	135.3(5)
Co1–P1	220.0(1)	220.5(2)	220.0(1)	220.7(3)	220.0(1)
Co1–P2	227.0(1)	220.6(2)	217.8(1)	218.7(2)	222.4(1)
Co1–P3	218.7(1)	219.4(2)	220.4(1)	220.8(3)	220.5(1)
O1–C6	125.2(4)	131.3(8)	131.1(5)	131(1)	129.8(4)
O2–C7	125.1(4)	131.1(8)	132.1(5)	132.8(9)	131.0(4)
O3–C10	–	–	–	–	142.7(5)
O4–C9	–	–	–	–	143.8(5)
C6–C7	149.9(7)	145(1)	144.2(6)	141(1)	143.3(5)
C7–C8	–	139(1)	138.5(7)	140(1)	140.3(5)
C8–C9	–		139.0(5)	139(1)	136.1(5)
C9–C10	–		144.2(6)	141(1)	141.4(5)
C10–C11	–		138.5(7)	140(1)	135.6(5)
C11–C6	–	139.2(9)	139.0(5)	139(1)	141.6(5)
C11–X	–	–	173.7(5)	190(2)	–
Co1–Co2 (Co1–C12)	520	759	756	758	705
O1–Co1–O2	83.0(1)	83.3(2)	84.2(1)	83.4(3)	83.2(1)
C6–O1–Co1	112.0(2)	113.9(4)	113.6(3)	113.6(6)	113.6(2)
C7–O2–Co1	111.7(2)	114.8(4)	113.0(3)	113.9(5)	114.0(2)
O1–C6–C7	116.7(4)	114.3(6)	114.2(4)	114.9(7)	114.5(3)
O2–C7–C6	116.5(4)	113.6(6)	114.2(4)	113.1(7)	114.5(3)
P1–Co1–P2	92.53(4)	91.33(7)	92.29(5)	91.47(9)	89.14(4)
P1–Co1–P3	90.15(5)	90.73(7)	90.77(5)	90.4(1)	90.36(4)
P2–Co1–P3	92.13(4)	90.26(7)	89.96(5)	90.6(1)	93.17(4)
P1–Co1–O1	93.13(9)	95.3(2)	89.8(1)	92.1(2)	91.45(8)
P1–Co1–O2	157.6(1)	148.3(2)	161.7(1)	153.2(2)	144.54(8)
P2–Co1–O1	104.4(1)	100.0(2)	111.5(1)	103.4(3)	101.18(9)
P2–Co1–O2	109.8(1)	120.2(2)	106.0(1)	115.3(2)	126.31(8)
P3–Co1–O1	163.0(1)	167.9(2)	158.5(1)	165.7(3)	165.56(9)
P3–Co1–O2	87.62(8)	86.1(2)	88.6(1)	88.0(2)	86.97(8)
O3–C12–O4	–	–	–	–	107.3(3)
C4–C1–P1–Co1	11.3	12.4	13.4	15.1	23.9
C4–C2–P2–Co1	10.0	13.4	7.9	15.6	34.1
C4–C3–P3–Co1	11.7	12.1	16.0	20.4	26.6
ligand/O1–Co1–O2-plane	0.3	4.3	8.3	8.8	7.6
ligand/O3–C12–O4-plane	–	–	–	–	8.3

[a] Estimated standard deviations of the least significant figures are given in parentheses.

The magnetic susceptibility of polycrystalline **1** was measured in the temperature range 10–290 K. The effective magnetic moment per dimer varies from 3.45 μ_B ($\chi T = 1.484$) at 290 K to 2.65 μ_B ($\chi T = 0.875$) at 10 K. The data in the temperature range 50–290 K follow a Curie–Weiss equation with a large negative Curie temperature ($\theta = -27.4\,°C$, $C = 1.59$).[18] Below 50 K the χ^{-1} versus T curve deviates substantially from a straight line. In principle this could be due to intermolecular antiferromagnetic interactions.[18] However, these interactions can be safely excluded in view of the crystal structure, in which the dimeric units are well separated. The deviation might therefore be due to intramolecular interactions. However, the magnetic data cannot be fitted satisfactorily to the Bleaney–Bowers equation for isotropic exchange in a $S = {}^1/_2/S = {}^1/_2$ dimer,[18] although the coupling constant $|2J|$ can be estimated as smaller than 10 cm^{-1}. Weak antiferromagnetic interactions have been observed previously in dinuclear (tripod)Co^{II} complexes with monoatomic bridges (e.g. Cl, Br, OH[14b] and SCH_3[19]) and multiatomic bridges of the 5,8-dihydroxy-1,4-naphthoquinone type.[20] The existence of a low-spin/high-spin equilibrium seems rather unlikely considering the EPR, UV/Vis and struc-

0947-6539/97/0305-0734 $ 17.50+.50/0 Chem. Eur. J. 1997, 3, No. 5

tural data for **1**, which compare well with other low-spin [(tripod)Co^{II}(L–L)] complexes (vide supra).

The spectroscopic, magnetic and structural data lead to the following description of **1**: the dinuclear dication consists of two low-spin cobalt(II) centres bridged by an oxalato dianion. The resulting two unpaired electrons are localised on the metal centres and show only a weak antiferromagnetic exchange interaction.

Structure and properties of 2a: The complex obtained with anilic acid (2,5-dihydroxy-1,4-benzoquinone) can be isolated after recrystallisation from methylene chloride as a deep-green microcrystalline analytically pure powder. Its FAB mass spectrum shows signals expected for the dinuclear composition (Table 4).

Compound **2a** crystallises with four CH_2Cl_2 solvate molecules per dimeric unit in the monoclinic centrosymmetric space group $P2_1/n$. A view of the dication of **2a** is depicted in Figure 4.

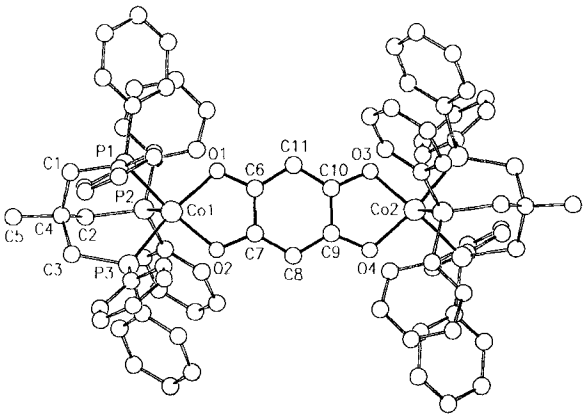

Figure 4. Perspective view of the dication of **2a** [49].

The solvate molecules and the counterions as well as the bulky tripod ligands isolate the dinuclear units such that the shortest interdimer Co–Co distance is 1300 pm. The intradimer metal–metal distance of 759 pm is determined by the geometry of the bridging ligand. The local geometry around each cobalt centre can be described as a distorted trigonal bipyramid with P3 and O1 occupying axial coordination sites. The bridging ligand is essentially planar but the two metal centres are located 10 pm above and below this plane, respectively. This results in a chair-type conformation of the Co-bridge-Co fragment with a dihedral angle between the ligand plane and the O-Co-O plane of 4.3°. The Co–O bond lengths of 189.8(5) and 188.3(5) pm in **2a** are identical within 3σ and differ significantly from the corresponding values in **1**. This reflects the different charge distribution in **2a** compared with **1**. On the other hand mononuclear complexes $[(tripod)Co^{III}(cat)]^+$ show Co–O bond lengths in the range 185–190 pm,[5] which are very similar to the values for **2a**, indicating a +III oxidation state of the cobalt ions in the present dinuclear complex. The structural features of the bridging ligand in **2a** are quite distinct from those encountered in **1**: the almost identical C–O bond lengths in **2a** are 6 pm shorter than those found in **1**. Compared with the dianions of chloranilic acid [124.3(6), 125.3(8) pm],[21] nitranilic acid [121.8(7), 122.1(7) pm][22] and complexes of anilic acid with copper (124–127 pm)[9], nickel [125.1(5), 126.5(5) pm][10] and rhodium [128(2), 126(2) pm],[12] the significantly longer C–O distances [131.1(8), 131.3(8) pm] in **2a** indicate the absence of a delocalised quinoid structure. Therefore the bridging ligand is poorly described by the dianionic (sq, sq) formulation (Figure 1) but better formulated as a tetraanionic (cat, cat) type or possibly as the trianionic (cat, sq) type. From structural comparisons alone the exact charge localised at the bridge cannot be obtained unambiguously because of the lack of structural data for the (cat, sq) and (cat, cat) types. For simplicity we will describe **2a** as a dinuclear Co^{III} complex bridged by a tetraanionic (cat, cat)-type ligand.

In accordance with this formulation **2a** is diamagnetic in solution and in the solid state. Therefore it is possible to obtain well-resolved ^1H NMR spectra (Figure 5). All signals expected

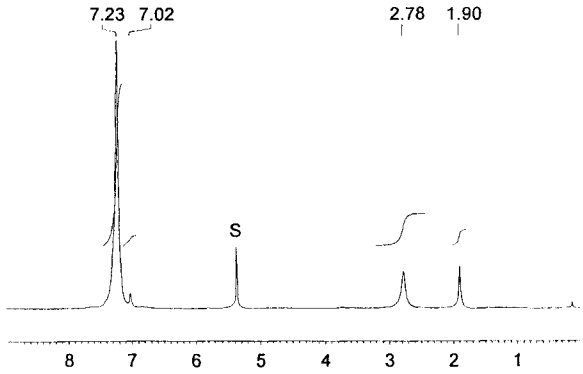

Figure 5. ^1H NMR spectrum of **2a** in CD_2Cl_2.

for the tripod ligand appear at characteristic chemical shifts and with correct intensity ratios. The two protons of the bridging ligand appear as a singlet at $\delta = 7.02$. This signal is significantly shifted to lower field compared with the free protonated ligand ($\delta = 5.81$ in [D_6]DMSO) and compared with the $[(bpy)_2Ru^{II}(sq, sq)Ru^{II}(bpy)_2]^{2+}$ complex ($\delta = 5.95$[13]) and the $[(cod)Rh^{I}(sq, sq)Rh^{I}(cod)]$ complex ($\delta = 5.23$[12]). This also confirms the more aromatic character of the bridging ligand in favour of the quinoid charge distribution.

Surprisingly no signal for the phosphorus atoms of the tripod ligand can be detected in the $^{31}P\{^1H\}$ NMR spectrum of **2a** at room temperature. Upon cooling to 190 K a broad signal appears at approximately $\delta = 29$, which gains sharpness and intensity on further cooling. The chemical shift lies in the typical range for $(tripod)Co^{III}$ complexes.[5] Dynamic behaviour as an explanation for this phenomenon, in the form of a pseudorotation of the tripod ligand, can definitely be excluded. If this applied, one singlet would be obtained in the temperature region of fast exchange owing to magnetic equivalence of the three phosphorus nuclei on the NMR timescale and three multiplets would arise in the slow exchange region.[23] The temperature dependence of the ^{31}P NMR signal of **2a** is clearly different. Another factor which could influence the linewidth of ^{31}P NMR signals is the quadrupole relaxation of the ^{31}P nuclei resulting from direct bonding to the ^{57}Co nucleus. In the thermal decoupling model,[24] relaxation of the phosphorus nuclei will be invoked by scalar coupling[25] between ^{31}P and ^{57}Co and modu-

lated by the quadrupole relaxation of the ^{57}Co. The linewidth therefore depends on the $^{1}J(^{31}P-^{57}Co)$ coupling constant and the longitudinal relaxation time of the cobalt nucleus. At low temperatures the ^{57}Co relaxation rate increases, the coupling to the ^{31}P will be suppressed (decoupling limit) and the linewidth will become smaller. This explanation could in principle be correct, although such a dynamic behaviour has never been observed in mononuclear (tripod)Co^{III} complexes. Therefore an explanation that involves the dinuclear structure and the special electronic configuration of **2a** would be more satisfactory. In order to quantify the ^{31}P NMR signal, compound **5a** (Figure 2) has been prepared. The phosphorus nuclei of the hexafluorophosphate counterions of **5a** serve as an internal standard for the integration of the tripod P signals.[26] Figure 6 shows the

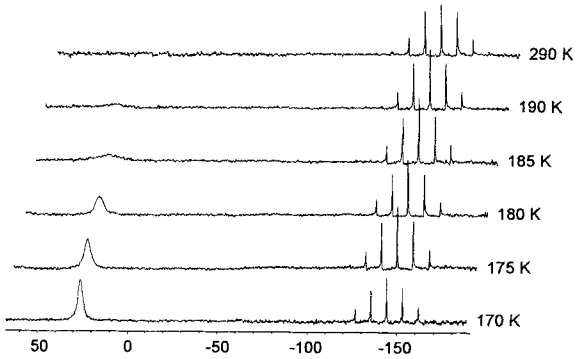

Figure 6. $^{31}P\{^{1}H\}$ NMR spectra of **5a** in CD_2Cl_2 at different temperatures.

temperature dependence of the $^{31}P\{^{1}H\}$ NMR spectra of **5a** (**2a** shows the same characteristics, though of course lacking the septet of the PF_6^- anion). At the lowest temperature reached (170 K) the integration ratio $P(PF_6)$:P(tripod) amounts to 1:2 (theoretically 1:3). Obviously the process has not gone to completion at this temperature. Additionally, the process is reproducible with different samples of **2a** (**5a**), reversible and independent of the counterion (BF_4^- in **2a**, PF_6^- in **5a**) and the solvent (methylene chloride, acetone). Therefore an intermolecular exchange process (e.g., solvent addition) can also be excluded. Changing the structure of the cationic part of the complex by substituting the hydrogens of the bridging ligand by chloride (**2b**), bromide (**2c**), iodide (**2d**), methyl (**2f**) or phenyl (**2h**) or substituting the phenyl groups of the tripod ligand by *p*-tolyl (**3**) or *m*-xylyl groups (**4**) leads to basically the same characteristics of the $^{31}P\{^{1}H\}$ NMR spectra except for the temperature at which the signal of the ^{31}P nuclei starts to appear. For **2b** (**5b**) the expected integration ratio $P(PF_6)$:P(tripod) of 1:3 can be reached at approximately 270 K. Therefore the dynamics must be caused by changes in the dication involving the metal centres. A possible, yet unprovable, explanation for the dynamics observed in the ^{31}P NMR spectra might be the existence of two distinct isomers in solution with different charge distributions within the dicationic molecule, for example a thermal equilibrium between the (cat, cat) and the (cat, sq) coordination modes (Figure 1) of the bridging ligand accompanying a Co^{III}/Co^{II} redox process. If just once during the NMR experiment (pulse and detection) this isomer exists—even for a very short time and therefore in very low macroscopic concentrations—the signal corresponding to the nearest neighbours of the cobalt centre, that is, the phosphorus nuclei, will be broadened owing to the paramagnetic relaxation. The macroscopic concentration might be too small to detect by static measurement techniques, such as susceptibility measurements. If this interpretation applies, the correspondence to the thermal equilibria of the type **B** compounds (Figure 1) with cobalt (+II, +III)[7] or manganese (+II, +III, +IV)[8] is then obvious.

Complex **2a** can be reduced electrochemically (Figure 7, Table 2) in two one-electron reduction steps (as confirmed by

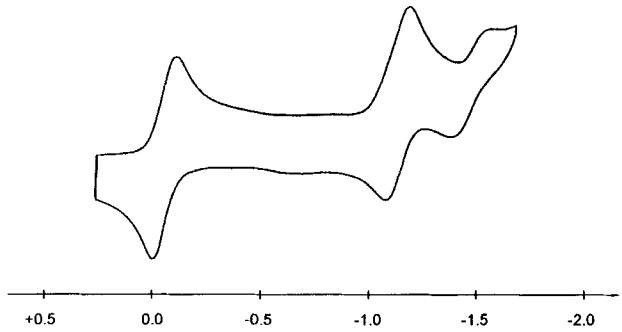

Figure 7. Cyclic voltammogram of **2a**.

Table 2. Electrochemical data for **2a**–**h**, **3** and **4** [a].

	$E_{1/2}(1)$ [a]	$E_{1/2}(2)$ [a]	K_C [b]
2a	−105	−1170	1.0×10^{18}
2b	+10	−1000	1.2×10^{17}
2c	+5	−1000	9.8×10^{16}
2d	±0	−995	6.6×10^{16}
2e	+170	−750	3.6×10^{15}
2f	−165	−1250	2.2×10^{18}
2g	−155	−1245	2.7×10^{18}
2h	−130	−1175	4.6×10^{17}
3	−150	(irr.)	–
4	−105	−1125	1.8×10^{17}

[a] In mV vs. SCE, 298 K. [b] 298 K.

electrolysis at a controlled potential of −0.11 V). The separation between the reduction waves of over 1 V corresponds to an equilibrium constant K_C [Eq. (2)] for the comproportionation [Eq. (1)] of the neutral and the dicationic to the monocationic complex of about 10^{18} (Table 2). This shows the high stability of the monocationic complex, which might be a result of

$$Co^{III}/Co^{III} + Co^{II}/Co^{II} \rightleftharpoons 2Co^{III}/Co^{II} \quad 2Co^{II^{1/2}}/Co^{II^{1/2}} \qquad (1)$$

$$K_c = \exp\left(\frac{\Delta E\ (\mathrm{mV})}{25.69}\right) \qquad T = 298\ \mathrm{K} \qquad (2)$$

delocalisation of the additional electron over the whole molecule, that is, over both metal centres and to some extent over the bridging ligand. In the Robin and Day classification of mixed-valence compounds,[27] this complex would hence belong to class III.

The EPR spectrum of the (electrochemically) singly reduced complex at 295 K shows a broad, poorly resolved signal centred at $g_{iso} \approx 2.11$. At 100 K in a microcrystalline methylene chloride

0947-6539/97/0305-0736 $ 17.50+.50/0 Chem. Eur. J. 1997, 3, No. 5

matrix, two g factors at $g_x = 2.28$ and $g_z = 2.01$ and coupling constants to the ^{57}Co nucleus of $A_x = 46$ and $A_z = 33$ G can be deduced. This indicates that the additional electron is mainly localised at the metal centres. The hyperfine splitting is smaller than the one found in mononuclear [(tripod)Co^{II}(cat)] complexes (A_x: 67–74, A_z: 48–53 G).[5a, 15] This might be caused by the delocalisation of the electron over both metal centres or by conformational differences in the coordination geometry around the metal centre in the dinuclear complex with respect to the mononuclear compound.

The electronic spectrum of **2a** (Figure 8, Table 3) contains several transitions in the visible and UV region. The most remarkable feature is the low-energy band at 1185 nm with an extinction coefficient $\varepsilon = 44000\,M^{-1}cm^{-1}$ (at 295 K). In order to investigate the low-temperature behaviour of **2a** a THF/CH_2Cl_2 solution (2:1) of **2a** was cooled to 100 K and the electronic spectra were recorded (Figure 8). Upon cooling, the intensity at the band maximum increases to almost $80000\,M^{-1}cm^{-1}$. As the band width at half height simultaneously decreases the integrated intensity (oscillator strength) remains essentially the same. In addition the NIR band shifts to lower energy ($\approx 150\,cm^{-1}$) at lower temperatures. As higher vibrational levels are depopulated at lower temperatures, a shift to higher energy is expected, which is found, for instance, for the [(tripod)Co^{III}(cat)]$^+$ complex[5b] ($\approx 500\,cm^{-1}$ for the 602 nm band and $\approx 200\,cm^{-1}$ for the 769 nm band in the same temperature range[28]). In complex **2a**, obviously, other effects compensate for and even surpass this vibrationally induced energy shift. In principle, one such effect could be a reordering of molecular orbitals inducing a different charge distribution within the molecule. This may also account for the unusual behaviour found in the ^{31}P NMR investigation. But at the current point of research all further interpretation would be speculative.

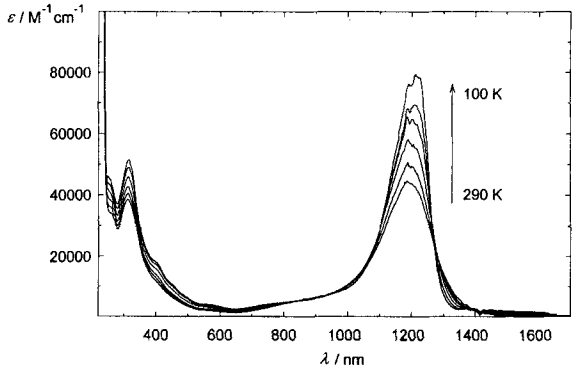

Figure 8. Electronic spectra of **2a** at different temperatures.

Table 3. UV/Vis/NIR data for **2a**–**h**, **3** and **4** [a].

	λ_{max} [nm] (log ε)				
2a	308 (4.46)	415 (3.73, sh)	591 (3.41)	844 (3.82, sh)	1185 (4.64)
2b	310 (4.43)	416 (3.88, sh)	595 (3.36)		1195 (4.76)
2c	310 (4.48)	413 (3.84, sh)	608 (3.43)		1195 (4.77)
2d	304 (4.57)	412 (3.76, sh)	476 (3.56)		1201 (4.57)
2e	304 (4.38)	435 (3.72, sh)	599 (3.40)		1187 (4.71)
2f	304 (4.40)	414 (3.75, sh)	563 (3.44)	855 (3.88, sh)	1152 (4.44)
2g	307 (4.29)	422 (3.79, sh)	563 (3.59)	865 (3.86, sh)	1132 (4.23)
2h	304 (4.46)	414 (3.81, sh)	580 (3.45, sh)	844 (3.81, sh)	1176 (4.63)
3	310 (4.39)	435 (3.75, sh)	591 (3.39)	849 (3.71, sh)	1181 (4.60)
4	307 (4.39)	416 (3.81, sh)	618 (3.40, sh)		1189 (4.74)

[a] In CH_2Cl_2.

The transition is slightly solvatochromic (maximum shift $750\,cm^{-1}$), with λ_{max} ranging from 1167 nm (acetonitrile) to 1279 nm (benzene).[29] This is in accordance with what would be expected for a transition with vectorial charge-transfer character. The observed shift to higher energy in more polar solvents must be due to a larger stabilisation of the ground state by polar solvents with respect to the excited state. The mononuclear [(tripod)Co(cat)]$^+$ complex behaves the same way: the CT bands are blue-shifted in polar solvents (150 and $400\,cm^{-1}$, respectively). The reverse case is found in [(bpy)Ru^{II}(sq, sq)Ru^{II}(bpy)]$^{2+}$:[13] the MLCT band $Ru^{II} \rightarrow$ ligand-π^* is shifted to lower energy in polar solvents. The ground state of the Ru complex is less polar than the excited state, therefore the excited state is stabilised in polar solvents and the energy gap decreases. The ground state of **2a**, however, is more polar than the excited state and so the ground state is stabilised in polar solvents, increasing the energy gap between these states.

The results of a molecular orbital calculation on the model compound [{$(PH_3)_3Co$}$_2(C_6H_2O_4)$]$^{2+}$ by the INDO method[30, 31] are presented in Figure 9. The in-phase combination (u with respect to the inversion centre) of the two CoL_3 centred orbitals[32] (in the staggered conformation) interacts with the b_{2u} orbital of the bridging ligand (in D_{2h} symmetry) to generate a low-lying filled orbital and the LUMO (b_u) of the complex (in C_{2h} symmetry). Mixing the out-of-phase combination (g) with the LUMO (b_{1g}) of the bridging ligand results in the formation of the HOMO (a_g) of the complex. The HOMO (b_{3g}) of the ligand remains nonbonding owing to symmetry mismatch. The ligand contributes the largest part of the HOMO of the complex (70%) and the remaining part is distributed between the two metal centres (15% each). In contrast the LUMO has mainly metal character (68%) and small ligand contributions. Therefore the HOMO $\rightarrow$ LUMO transition has considerable LMCT character. A CI calculation[33] indicates that the intense absorption band in the electronic spectrum of **2a** is mainly composed of this HOMO $\rightarrow$ LUMO transition. The charge-transfer character and the fact that this transition is al-

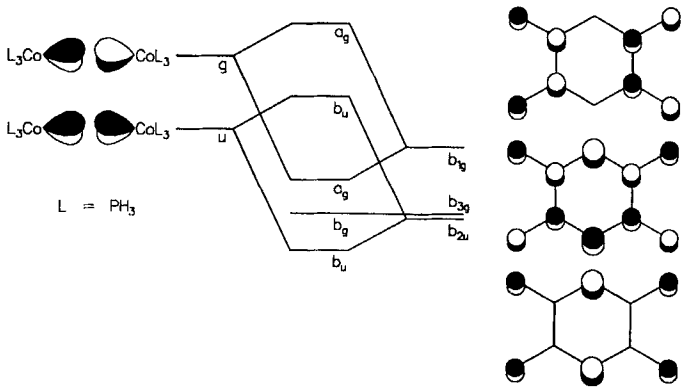

Figure 9. Orbital interaction diagram for [{$(PH_3)_3Co)_2(C_6H_2O_4)$}]$^{2+}$. The splitting of the g/u combinations is exaggerated for clarity.

lowed by symmetry (HOMO: a_g, LUMO: b_u) give rise to a large transition dipole moment and thus to a high intensity of the corresponding absorption band. The second result of the calculation is that in terms of the INDO model the charge distribution of the ground state of the dication is best described as Co^{III}–(cat, cat)–Co^{III} with some charge delocalisation onto the metals. Furthermore, the metal character of the LUMO agrees very well with the EPR results for the singly reduced complex and the higher polarity of the ground state (Co^{III}–(cat, cat)–Co^{III}) with respect to the excited state ($Co^{II1/2}$–(cat, sq)–$Co^{II1/2}$) is in accordance with the observed solvatochromic shift of the LMCT absorption band to higher energy in polar solvents (vide supra).

Influence of substituents at the bridging ligand: Reaction of 3,6-disubstituted 2,5-dihydroxy-1,4-benzoquinones with (tripod)-cobalt(II) fragments afforded the dark green compounds **2b–h** (Figure 2). All complexes were characterised by elemental analyses and FAB mass spectroscopy (Table 4). Single crystals

Table 4. FAB-MS data for **1**, **2a–h**, **3**, **4** and **5a** [a].

	$[M^{2+}+X^-]$	$[M^+]$	[(tripod)CoL + Ph + f]$^+$	[(tripod)-CoL]$^+$	$[M^{2+}]$
1	1543 (25)	1457 (100)	850 (34)	–	728 (88)
2a	1591 (5)	1504 (30)	899 (5)	821 (12)	752 (100)
2b	1659 (15)	1574 (100)	967 (10)	890 (2)	787 (63)
2c	1747 (18)	1660 (100)	1056 (12)	977 (6)	831 (50)
2d	1843 (20)	1756 (100)	1151 (32)	1074 (8)	878 (60)
2e	1679 (10)	1594 (100)	988 (3)	912 (2)	797 (54)
2f	1619 (18)	1532 (100)	927 (85)	849 (12)	766 (18)
2g	1677 (18)	1589 (100)	983 (25)	907 (14)	794 (65)
2h	1742 (28)	1655 (100)	1051 (16)	973 (8)	828 (78)
3	1760 (18)	1671 (100)	983 (10)	905 (8)	836 (45)
4	1998 (15)	1911 (100)	1136 (12)	1058 (5)	955 (52)
5a	1648 (60)	1504 (100)	899 (90)	821 (20)	752 (44)

[a] m/z (%), M = cation, X^- = PF_6^- for **5a**, otherwise BF_4^-, L = bridging ligand.

of **2b**, **2c** and **2e** were obtained by slow diffusion of diethyl ether into dilute solutions of the complexes in acetone, acetonitrile and acetone, respectively. All dications have bonding characteristics similar to compound **2a** (Table 1). The structure of **2e** could be solved but not refined because of decomposition of the crystal during the data collection. Therefore details of the structure of **2e** are not given. Just one feature of the bridging ligand of **2e** should be noted: the planes of the NO_2 groups of the ligand are not coplanar with the ligand plane. Likewise in the solid state the nitro groups of nitranilic acid and the nitranilate dianion were found to be twisted around the C–N bond by 22°[22] and 6°,[34] respectively.

Like complex **2a**, the complexes **2b–h** can be reduced in two reversible reduction steps (Table 2) and all show a strong absorption band in the NIR of the electronic spectrum (Table 3). The reduction potentials reveal that electron-withdrawing substituents (halogens) faciliate the reduction of the metal centres while electron-donating substituents (alkyls) render it more difficult. Also the energy of the LMCT absorption depends on the substitution pattern of the bridging ligand: electron-withdrawing substituents induce a red shift, while electron-donating substituents shift the band to higher energy. In the MO scheme (Figure 9) both the HOMO and the LUMO of the complex are affected by energy changes of the ligand orbitals (b_{2u} and b_{1g}) relative to the orbital energies of the L_3Co fragments because of orbital mixing of the metal d_π orbitals and ligand orbitals in the complex.

The correlation of the energy of the electronic transition with the two reduction potentials is shown in Figure 10. Except in

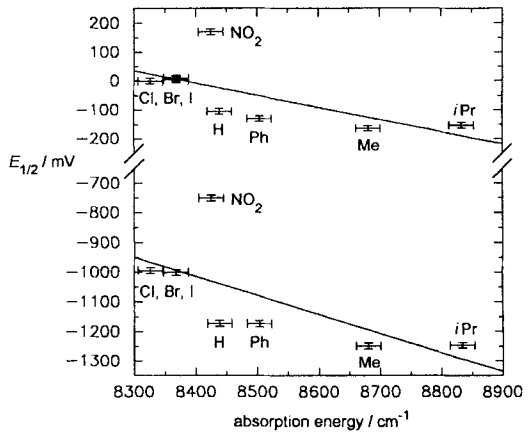

Figure 10. Plot of reduction potentials vs. absorption energy for **2a–h** (substituents respectively H, Cl, Br, I, NO_2, Me, *i*Pr, Ph).

the case of complex **2e**, fairly linear correlations are obtained. This relationship confirms the CT character of the absorption band: the easier the reduction of the cobalt(III) centres to the "$+II^1/_2$" and +II oxidation states, the lower the energy of the absorption band. Both reduction potentials show the same behaviour; this suggests that both electrons enter the same molecular orbital (LUMO). As the LUMO is a metal-centred orbital, successive reduction leads first to the monocationic $Co^{II1/2}$/$Co^{II1/2}$ complex, then to the neutral Co^{II}/Co^{II} complex. The comproportionation constants K_C [Eq. (2)] are listed in Table 2. In all cases the mixed valence species are very stable towards disproportionation. This stabilisation is due to the delocalisation of the unpaired electron over both metals and to a smaller extent over the bridging ligand.

To confirm the statement that the reduction of the complexes is a mainly metal-centred process and that the ligand plays only a minor role, the dependence of the reduction potential of the free ligand on the substituent has been elucidated. The reduction of the ligand is unfortunately accompanied by proton transfer reactions so that the reduction waves appear only as quasireversible waves. Therefore the peak potential E_p of the reduction process is used. The potentials of both the complex and the ligand can be correlated with the Hammett substituent parameter[35] as shown in Figure 11. The straight lines are calculated by the least-squares method. The slope of the line for the complexes is significantly smaller than the slope of the line for the ligands, indicating that the dependence of the reduction potential on the substituents is much smaller in the complexes than in the uncomplexed ligands and confirming that the reduction of the complexes is not ligand- but metal-centred.

Compound **2e** deserves further comment as the electrochemical and optical data do not fit well into this picture. As observed in the solid state, the nitro groups are not coplanar with the

0947-6539/97/0305-0738 $ 17.50+.50/0 Chem. Eur. J. 1997, 3, No. 5

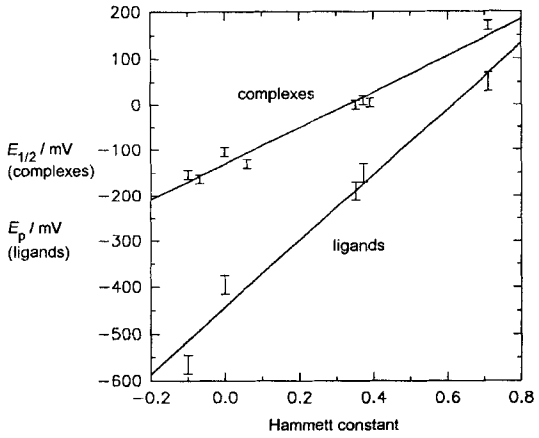

Figure 11. Hammett plot of the reduction potentials of the ligands and complexes.

plane of the bridging ligand, and electron delocalisation onto the nitro groups by mesomeric effects should thus be small. In solution, however, rotation of the nitro groups should be possible and charge distribution onto the NO_2 moiety could take place. MO calculations for a model complex for **2e** with coplanar nitro groups indicate that both HOMO and LUMO have significant density on the nitro groups. This stabilises both the HOMO and the LUMO, thereby hardly affecting the energy of the absorption band but significantly lowering the reduction potentials.

Influence of substituents at the tripod ligand: With alkylated tripod ligands instead of the hexaphenyl tripod ligand, the syntheses of the complexes yielded compounds **3** (X = H, tripod = $CH_3C(CH_2P(p\text{-tolyl})_2)_3$) and **4** (X = Cl, tripod = $CH_3C(CH_2P(m\text{-xylyl})_2)_3$) (Figure 2). Both complexes were characterised by FAB mass spectroscopy (Table 4), elemental analyses and NMR spectroscopy. The ^{1}H NMR spectrum of **3** is shown in Figure 12. The signals of the tripod ligand appear at expected

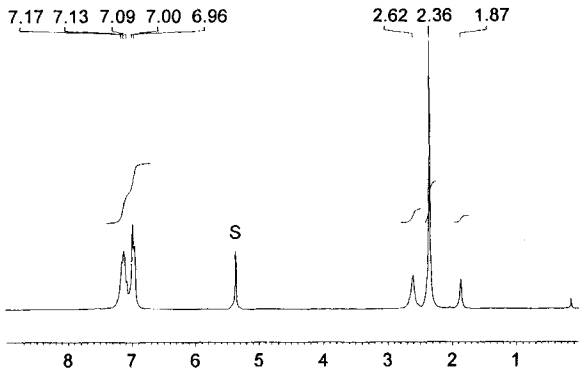

Figure 12. ^{1}H NMR spectrum of **3** in CD_2Cl_2.

positions, with correct intensity ratios and expected coupling patterns. The protons of the bridging ligand give rise to a singlet at $\delta = 7.09$, which, as in the case of **2a**, lies in the aromatic region.

Electrochemical and UV/Vis/NIR data are compiled in Tables 2 and 3, respectively. Methyl groups in the *p*-positions of the six aromatic rings of the tripod ligand in **3** shift the first reduction potential (the second reduction process of **3** is irreversible) to a more negative value relative to that of **2a** (shift 45 mV) and cause a marginal blue shift of the energy of the absorption band ($\approx 30\ cm^{-1}$). Introduction of two methyl groups per phenyl ring (in the *m*-positions) in the tripod ligand (**4**) gives rise to the following changes compared with the spectrum of **2b**: the two reduction processes of **4** appear at more negative potentials (shift ≈ 120 mV) and the peak maximum of the absorption band is slightly shifted to higher energy ($\approx 40\ cm^{-1}$). These small effects can be easily explained by means of the MO picture derived in the previous paragraphs. The more electron-donating alkylated tripod ligands raise the energy of the metal-centred orbitals (the LUMO of the complex) while leaving the energy of the bridging ligand orbitals (the HOMO of the complex) relatively unaffected. This results in a slightly larger HOMO–LUMO gap of the complexes **3** and **4** and thus in a small blue shift of the absorption bands. The higher-lying LUMO of the methylated complexes renders the reduction processes more difficult, thus shifting the reduction potentials to more negative values. The effects observed for **3** and **4**, though small, are consistent with the proposed model of charge distribution in the ground state.

Comparison with mononuclear complexes: In order to understand the strong metal–metal interaction mediated by the bridging ligands in the dinuclear complexes which manifests itself, for example, in the large comproportionation constants for the mixed-valence state[36] the mononuclear model compound **6** (Figure 2) has been prepared. In **6** one "[(tripod)cobalt(III)]$^{3+}$" fragment has been replaced formally by a methylene group ("$[CH_2]^{2+}$"). Compound **6** can be isolated as a turquoise complex crystallised with half a methylene chloride per molecule. The molecular structure is confirmed by an X-ray structural analysis (Figure 13). The C–C, C–O, Co–O and Co–P distances (Table 1) compare well with those found in other [(tripod)Co(cat)]$^+$ complexes.[5] Remarkably, neither the O-Co-O plane nor the O-CH_2-O plane lies in the plane of the six-membered ring (Table 1); instead they are bent in such a way that a boatlike conformation results (in the dinuclear compounds a chairlike conformation was observed).

The ^{31}P{^{1}H} NMR spectrum consists of a singlet at $\delta = 35.6$. This pattern does not vary over the temperature range 295–200 K and is consistent with the behaviour of other five-coordi-

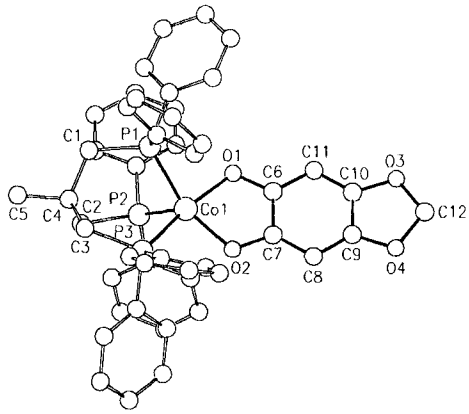

Figure 13. Perspective view of the cation of **6** [49].

nate (tripod)Co^{III} complexes, which all show a rapid intramolecular exchange of the three phosphorus atoms of the tripod ligand on the NMR timescale.[5]

The turquoise colour of **6** arises from two strong absorption bands in the visible region of the electronic spectrum at 673 nm ($\varepsilon = 6980\,M^{-1}cm^{-1}$) and 796 nm ($\varepsilon = 13450\,M^{-1}cm^{-1}$) (Figure 14). These bands are red-shifted by 1750 and 440 cm^{-1}, respectively, with respect to the unsubstituted [(tripod)Co(cat)]$^+$ complex.[5b] The intensity of the low-energy band increases by a factor of 1.8, the intensity of the high-energy band by a factor of 1.3 (Figure 14).

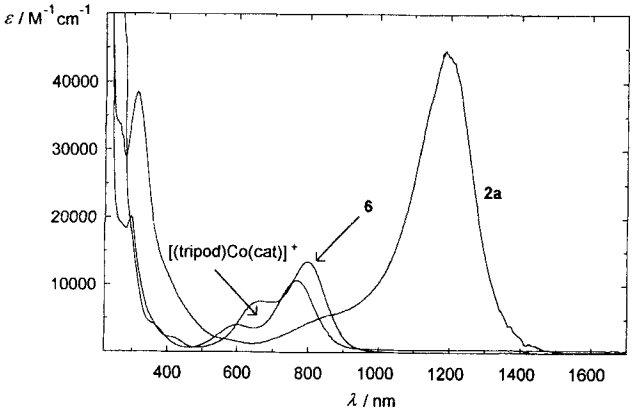

Figure 14. Comparison of the electronic spectra of **2a**, **6** and [(tripod)Co(cat)]$^+$.

It has been shown by EHMO calculations that the HOMO of the [(tripod)Co(cat)]$^+$ complexes is mainly centred on the catecholato ligand and that the LUMO is localised at the cobalt centre.[5a] This was also confirmed by EPR spectroscopy of the corresponding reduced Co^{II} catecholato species.[5a, 15] For comparison with the dinuclear complexes, the interaction diagram for the mononuclear model compound $[(PH_3)_3Co(C_6H_4O_2)]^+$ calculated with the INDO method[30] is presented in Figure 15.

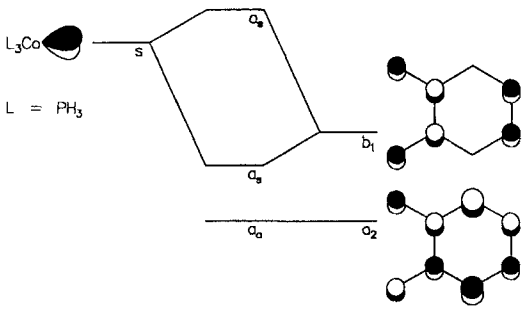

Figure 15. Orbital interaction diagram for $[((PH_3)_3Co)(C_6H_4O_2)]^+$.

The symmetry labels of the ligand belong to the C_{2v} point group, and the index s of the L_3Co fragment refers to the mirror plane perpendicular to the plane of the diagram (C_S point group). The HOMO (b_1) of the catecholato ligand has the correct symmetry to interact with the orbital of the L_3Co fragment (s) resulting in a Co–O bonding, mainly ligand-centred, MO and a Co–O antibonding, mainly metal-centred, MO. The a_2 MO of the ligand remains nonbonding. These results are consistent with the previous EHMO calculations.[5a] A CI calculation[37] reveals that the low-energy absorption band of the complex is mainly due to the HOMO → LUMO transition, while the less intense high-energy band corresponds to the (HOMO − 1) → LUMO excitation. As the HOMO and the (HOMO − 1) have large ligand character and as the LUMO is strongly metal-centred, the transitions are both of the LMCT type. The charge-transfer character of the absorption bands of [(tripod)Co^{III}(o-(X)(Y)C_6H_4)]$^+$ complexes (X, Y = O, S, NH) has already been demonstrated.[5b]

The interaction diagram of the dinuclear complex (Figure 9) is basically very similar to the diagram of the mononuclear complex (Figure 15). However, in the dinuclear case there is a second interaction of the L_3Co fragments with the ligand: the u-combination of the metal fragments mixes with the b_{2u} orbital of the ligand, thereby forming the b_u MO (LUMO) of the complex. This orbital is inserted between the HOMO and the LUMO of the mononuclear complex and reduces the HOMO–LUMO gap considerably, thus leading to a large shift of the CT band to lower energy. The fact that the LUMO of the dinuclear complex lies at a considerably lower energy is also reflected in the reduction potentials: the mononuclear complex **6** is reduced at 0.56 V, which is comparable to other [(tripod)Co(cat)]$^+$ complexes; the dinuclear complex **2a**, however, can be reduced at only −0.11 V.

As confirmed by the reduction potentials and the electronic spectrum, the methylenedioxo group in **6** induces only a small perturbation with respect to the unsubstituted [(tripod)Co(cat)]$^+$ complex (observed red shifts 1750 and 440 cm^{-1}, respectively). On the other hand the second (tripod)cobalt moiety in the dinuclear complexes does not act as a simple substituent but drastically changes the electronic properties (observed red shift 4570 cm^{-1}). The interaction between the two metal centres is transmitted by the bridging ligand orbitals (Figure 9: b_{1g}, b_{2u}), which have appropriate symmetry to mix with the metal orbitals.

Conclusions

The present study of dinuclear complexes with two redox-active metal centres and one "non-innocent" bridging tetrox ligand has illustrated that it is possible to generate the previously unknown charge distribution of the (cat, cat) type (Figure 1) in dinuclear complexes. This has been accomplished by transferring two electrons from the two (tripod)Co^{II} fragments to the (sq, sq)-type ligand (Figure 1). The bridging (formally aromatic) ligand provides a communication channel between the metal centres, as shown by the large splitting of the two reduction potentials giving rise to a high stability of the singly reduced (mixed-valence) complexes. The unique spectral features and redox properties of the dinuclear complexes are explained within a qualitative MO model. These properties can be tuned by substitutions at the bridging ligand and at the tripod ligand.

Experimental Section

All manipulations were carried out under an inert atmosphere by means of standard Schlenk techniques. All solvents were dried by standard methods and distilled under inert gas. NMR: Bruker AC200 at 200.13 MHz (^1H),

© VCH Verlagsgesellschaft mbH, D-69451 Weinheim, 1997 0947-6539/97/0305-0740 $ 17.50+.50/0 Chem. Eur. J. 1997, 3, No. 5

50.323 MHz ($^{13}C\{^1H\}$), 81.015 MHz ($^{31}P\{^1H\}$); chemical shifts (δ) in ppm with respect to CD_2Cl_2 (^1H: $\delta = 5.32$, ^{13}C: $\delta = 53.5$) and [D$_6$]acetone (^1H: $\delta = 2.04$, ^{13}C: $\delta = 29.8$) as internal standards and to H_3PO_4 (^{31}P: $\delta = 0$) as external standard. IR: Bruker FTIR IFS-66, as CsI disks. UV/Vis/NIR: Perkin Elmer Lambda 19, Oxford temperature control unit ITC-4, Oxford cryostat DN-1704. MS (FAB): Finnigan MAT 8230, 4-nitrobenzyl alcohol matrix. EPR: Bruker ESP 300 E, X-band, standard cavity ER 4102, temperature control unit Eurotherm B-VT 2000, external standard diphenylpicrylhydrazyl (DPPH). Elemental analyses: microanalytical laboratory of the Organisch-Chemisches Institut, Universität Heidelberg. Melting points (not corrected): Gallenkamp MFB-595 010. Cyclic voltammetry: Metrohm Universal Mess- und Titriergefäss, Metrohm GC electrode RDE 628, platinum electrode, SCE electrode, Princeton Applied Research potentiostat Model 273, 10^{-3} M in 0.1 M nBu_4NPF_6/CH_3CN. Electrolyses: basically equipment as before, platinum grid as working electrode, zinc bar as counterelectrode. Magnetic measurements: a) Faraday balance: Bruker electromagnet B-E 15 C8, Bruker field controller B-H 15, Sartorius vacuum-micro balance M 25 D-S, Oxford temperature control unit ITC-4, Oxford He-evaporator cryostat CF 1200, calibration with $K_3[Fe(CN)_6]$; b) Evans method: calibration with diphenylpicrylhydrazyl (DPPH).[38]

Chemicals: Oxalic acid $C_2H_2O_4$, anilic acid $C_6H_4O_4$, chloranilic acid $C_6H_2O_4Cl_2$ are commercially available. Anilic acid was sublimed before use (400 K, 0.01 mbar). Other ligands were prepared by published procedures: 1,1,1-tris(diphenylphosphanomethyl)ethane $CH_3C(CH_2PPh_2)_3$,[39] 1,1,1-tris(di-(*p*-tolyl)phosphanomethyl)ethane $CH_3C(CH_2P(p\text{-tolyl})_2)_3$,[40] 1,1,1-tris(di-(*m*-xylyl)phosphanomethyl)ethane $CH_3C(CH_2P(m\text{-xylyl})_2)_3$,[40] 4,5-methylenedioxo-1,2-benzoquinone $C_7H_4O_4$,[41] 2,5-dihydroxy-3,6-dibromo-1,4-benzoquinone $C_6H_2O_4Br_2$,[42] 2,5-dihydroxy-3,6-diiodo-1,4-benzoquinone $C_6H_2O_4I_2$,[43] 2,5-dihydroxy-3,6-dinitro-1,4-benzoquinone $C_6H_2O_4(NO_2)_2$,[44] 2,5-dihydroxy-3,6-dimethyl-1,4-benzoquinone $C_6H_2O_4(CH_3)_2$,[45] 2,5-dihydroxy-3,6-diisopropyl-1,4-benzoquinone $C_6H_2O_4(CH(CH_3)_2)_2$,[46] 2,5-dihydroxy-3,6-diphenyl-1,4-benzoquinone $C_6H_2O_4(C_6H_5)_2$.[47]

(μ-Oxalato)bis[{1,1,1-tris(diphenylphosphanomethyl)ethane}cobalt]bis(tetrafluoroborate) (1): A solution of $[Co(BF_4)_2]\cdot 6H_2O$ (341 mg, 1 mmol) in ethanol (15 mL) was added to a solution of the tripod ligand (624 mg, 1 mmol) in THF (15 mL). Addition of oxalic acid (45 mg, 0.5 mmol) to the orange-red coloured solution caused a slow colour change to red-brown. After the solution had been stirred for two hours it was filtered. The reaction mixture was concentrated in vacuo until **1** started to precipitate. The precipitate was filtered off, washed with cold ethanol (10 mL) and twice with diethyl ether (10 mL portions). The microcrystalline product was recrystallised from methylene chloride/diethyl ether (yield 670 mg, 82%). Vapour diffusion of diethyl ether into a methylene chloride solution of the complex afforded red-brown crystals suitable for X-ray crystallographic analysis. M.p. = 320 °C (decomp.); IR (CsI): $\tilde{\nu} = 1637\ cm^{-1}$ (s), 1483 (m), 1436 (s), 1337 (w), 1282 (w), 1192 (w), 1160 (w), 1096 (s), 1059 (br), 998 (m), 834 (w), 739 (m), 695 (s); UV/Vis/NIR (CH_2Cl_2): λ_{max} (ε, $M^{-1}cm^{-1}$) = 313 nm (18 500), 481 nm (1180), 919 nm (120); $C_{84}H_{78}P_6O_4Co_2B_2F_8$ (1628.9): calcd. C 61.94, H 4.83, P 11.41; found C 61.70, H 4.91, P 11.21.

(μ-X-Anilato)bis[{1,1,1-tris(diphenylphosphanomethyl)ethane}cobalt]bis(tetrafluoroborate) (2a–h): A solution of $[Co(BF_4)_2]\cdot 6H_2O$ (341 mg, 1 mmol) in ethanol (15 mL) was added to a solution of the tripod ligand (624 mg, 1 mmol) in THF (15 mL). Addition of the coligand (X = H: 70 mg; X = Cl: 105 mg; X = Br: 149 mg; X = I: 196 mg; X = NO_2: 115 mg; X = Me: 84 mg; X = *i*Pr: 112 mg; X = Ph: 146 mg, 0.5 mmol) to the orange-red coloured solution caused an immediate colour change to dark green. After the mixture had been stirred for one hour the precipitated complex was filtered off, washed with diethyl ether (2 × 10 mL), cold ethanol (2 × 10 mL) and again diethyl ether (2 × 10 mL). The compounds were recrystallised from methylene chloride/diethyl ether (yields ranged from 60–80%). Crystals suitable for X-ray crystallographic analyses were obtained by vapour diffusion of diethyl ether into a dilute solution of the complex salts (**2a**: methylene chloride, **2b**: acetone, **2c**: acetonitrile, **2e**: acetone).

2a: M.p. 320 °C (decomp.); IR (CsI): $\tilde{\nu} = 3059\ cm^{-1}$ (m), 1584 (m), 1573 (m), 1483 (m), 1435 (s), 1275 (m), 1095 (s), 1050 (br), 998 (m), 818 (w), 739 (s), 691 (s); ^1H NMR (CD_2Cl_2): $\delta = 1.90$ (s, 3H, CH_3), 2.78 (brs, 6H, CH_2), 7.02 (s, 1H, ligand-CH), 7.2 (brs, 30H, CH_{ar}); $^{31}P\{^1H\}$ (CD_2Cl_2): $\delta = 29$ (brs) (190 K); $C_{88}H_{80}P_6O_4Co_2B_2F_8$ (1678.9): calcd. for **2a**·0.5CH_2Cl_2: C 61.75, H 4.74; found C 61.71, H 4.92.

2b: M.p. 315 °C (decomp.); IR (CsI): $\tilde{\nu} = 3060\ cm^{-1}$ (m), 1584 (m), 1572 (m), 1482 (m), 1435 (s), 1390 (m), 1276 (m), 1094 (s), 1056 (br), 998 (m), 863 (m), 818 (w), 740 (s), 692 (s); ^1H NMR ([D$_6$]acetone): $\delta = 1.83$ (s, 3H, CH_3), 2.65 (brs, 6H, CH_2), 7.0–7.3 (m, 30H, CH_{ar}); ^1H NMR (CD_2Cl_2): $\delta = 2.02$ (s, 3H, CH_3), 2.71 (brs, 6H, CH_2), 7.1–7.4 (m, 30H, CH_{ar}); $^{31}P\{^1H\}$ ([D$_6$]acetone): $\delta = 35$ (brs) (285 K); $C_{88}H_{78}P_6O_4Cl_2Co_2B_2F_8$ (1747.8): calcd. for **2b**·0.5CH_2Cl_2: C 59.21, H 4.72; found C 59.20, H 4.67.

2c: M.p. 307 °C (decomp.); IR (CsI): $\tilde{\nu} = 3056\ cm^{-1}$ (m), 1586 (m), 1573 (m), 1480 (m), 1435 (s), 1386 (m), 1273 (m), 1094 (s), 1049 (br), 995 (m), 822 (w), 816 (w), 739 (s), 690 (s); ^1H NMR (CD_2Cl_2): $\delta = 1.80$ (s, 3H, CH_3), 2.61 (brs, 6H, CH_2), 7.0–7.3 (m, 30H, CH_{ar}); $^{31}P\{^1H\}$ (CD_2Cl_2): $\delta = 30$ (brs) (220 K); $C_{88}H_{78}P_6O_4Br_2Co_2B_2F_8$ (1836.7): calcd. for **2c**·2.5CH_2Cl_2: C 52.92, H 4.32; found C 52.65, H 4.18.

2d: M.p. 249 °C (decomp., loss of I_2); IR (CsI): $\tilde{\nu} = 3060\ cm^{-1}$ (m), 1584 (m), 1573 (m), 1483 (m), 1435 (s), 1378 (m), 1282 (m), 1095 (s), 1052 (br), 996 (m), 834 (m), 818 (m), 804 (w), 741 (s), 691 (s); ^1H NMR (CD_2Cl_2): $\delta = 1.81$ (s, 3H, CH_3), 2.59 (brs, 6H, CH_2), 7.1–7.3 (m, 30H, CH_{ar}); $^{31}P\{^1H\}$ (CD_2Cl_2): $\delta = 30$ (brs) (220 K); $C_{88}H_{78}P_6O_4I_2Co_2B_2F_8$ (1930.7): calcd. for **2d**·1.0CH_2Cl_2: C 52.90, H 4.24; found C 52.40, H 4.62.

2e: M.p. 290 °C (decomp.); IR (CsI): $\tilde{\nu} = 3059\ cm^{-1}$ (m), 1584 (m), 1573 (m), 1529 (s), 1483 (m), 1435 (s), 1365 (m), 1282 (s), 1191 (m), 1093 (s), 1051 (br), 996 (m), 834 (w), 816 (w), 741 (s), 692 (s); $C_{88}H_{78}P_6O_8N_2Co_2B_2F_8$ (1768.9): calcd. for **2e**·0.5CH_2Cl_2 C 58.52, H 4.66, N 1.54; found C 58.46, H 4.76, N 1.47.

2f: M.p. 280 °C (decomp.); IR (CsI): $\tilde{\nu} = 3064\ cm^{-1}$ (m), 1586 (m), 1573 (m), 1482 (m), 1435 (s), 1391 (w), 1273 (m), 1189 (m), 1097 (s), 1057 (br), 998 (m), 836 (w), 817 (w), 740 (s), 695 (s); ^1H NMR (CD_2Cl_2): $\delta = 1.83$ (s, 3H, CH_3), 2.50 (brs, 3H, ligand-CH_3), 2.69 (brs, 6H, CH_2), 7.1 (brs, 30H, CH_{ar}); $^{31}P\{^1H\}$ (CD_2Cl_2): $\delta = 27$ (brs) (210 K); $C_{90}H_{84}P_6O_4Co_2B_2F_8$ (1707.0): calcd. for **2f**·1.5CH_2Cl_2: C 59.75, H 5.04; found C 59.74, H 5.15.

2g: M.p. 285 °C (decomp.); IR (CsI): $\tilde{\nu} = 3057\ cm^{-1}$ (m), 1604 (m), 1484 (m), 1435 (s), 1356 (m), 1275 (m), 1188 (m), 1095 (s), 1056 (br), 998 (m), 833 (w), 815 (w), 739 (s), 694 (s); $C_{94}H_{92}P_6O_4Co_2B_2F_8$ (1763.1): calcd. for **2g**·1.0CH_2Cl_2: C 61.74, H 5.31; found C 61.15, H 5.58.

2h: M.p. > 300 °C (decomp.); IR (CsI): $\tilde{\nu} = 3052\ cm^{-1}$ (m), 1599 (m), 1480 (m), 1434 (s), 1388 (w), 1275 (m), 1188 (m), 1094 (s), 1057 (br), 998 (m), 837 (w), 815 (w), 738 (s), 692 (s); ^1H NMR (CD_2Cl_2): $\delta = 1.89$ (s, 3H, CH_3), 2.52 (brs, 6H, CH_2), 6.9–7.8 (m, 35H, CH_{ar}); $^{31}P\{^1H\}$ (CD_2Cl_2): $\delta = 28$ (brs) (200 K); $C_{100}H_{88}P_6O_4Co_2B_2F_8$ (1831.1): calcd. for **2h**·1.5CH_2Cl_2: C 62.25, H 4.68; found C 62.63, H 5.00.

(μ-Anilato)bis[{1,1,1-tris(di(*p*-tolyl)phosphanomethyl)ethane}cobalt]bis(tetrafluoroborate) (3): A solution of $[Co(BF_4)_2]\cdot 6H_2O$ (341 mg, 1 mmol) in ethanol (15 mL) was added to a solution of the tripod ligand (708 mg, 1 mmol) in THF (15 mL). Addition of anilic acid (70 mg, 0.5 mmol) to the orange-red coloured solution caused an immediate colour change to dark green. After the mixture had been stirred for one hour the precipitated complex salt was filtered off, washed with diethyl ether (2 × 10 mL), cold ethanol (2 × 10 mL) and again diethyl ether (2 × 10 mL). **3** was recrystallised from methylene chloride/diethyl ether (600 mg, 65%); M.p. 285 °C (decomp.); IR (CsI): $\tilde{\nu} = 3023\ cm^{-1}$ (m), 2965 (m), 1596 (m), 1500 (m), 1395 (m), 1269 (w), 1191 (m), 1094 (s), 1057 (br), 1016 (m), 801 (m), 758 (w), 734 (m), 706 (w), 619 (m); ^1H NMR (CD_2Cl_2): $\delta = 1.87$ (s, 3H, CH_3), 2.36 (s, 18H, Ph-CH_3), 2.62 (brs, 6H, CH_2), 6.98 (d, $^3J_{HH} = 6.6$ Hz, 12H, CH_{ar}), 7.15 (d, $^3J_{HH} = 6.6$ Hz, 12H, CH_{ar}), 7.09 (s, 1H, ligand-CH); $^{31}P\{^1H\}$ (CD_2Cl_2): $\delta = 30$ (brs) (215 K); $C_{88}H_{80}P_6O_4Co_2B_2F_8$ (1847.2): calcd. for **3**·2.5CH_2Cl_2: C 59.78, H 5.33; found C 59.56, H 5.30.

(μ-Chloranilato)bis[{1,1,1-tris(di(*m*-xylyl)phosphanomethyl)ethane}cobalt]bis(tetrafluoroborate) (4): A solution of $[Co(BF_4)_2]\cdot 6H_2O$ (341 mg, 1 mmol) in ethanol (15 mL) was added to a solution of the tripod ligand (792 mg, 1 mmol) in THF (15 mL). Addition of chloranilic acid (104 mg, 0.5 mmol) to the orange-red coloured solution caused an immediate colour change to dark green. After the mixture had been stirred for one hour the precipitated complex salt was filtered off, washed with diethyl ether (2 × 10 mL), cold ethanol (2 × 10 mL) and again diethyl ether (2 × 10 mL). Compound **4** was recrystallised from methylene chloride/diethyl ether (854 mg, 82%); M.p. 302 °C (decomp.); IR (CsI): $\tilde{\nu} = 2919\ cm^{-1}$ (m), 1605 (m), 1484 (m), 1420 (s), 1303 (w), 1275 (w), 1130 (m), 1096 (s), 1050 (br), 993 (m), 845 (m), 816 (w), 763 (w), 740 (w), 692 (m); ^1H NMR (CD_2Cl_2): $\delta = 1.94$ (s, 3H, CH_3), 2.05 (s, 36H, Ph-CH_3), 2.57 (brs, 6H, CH_2), 6.88 (s, 6H, *p*-CH_{ar}), 6.98 (s, 12H,

o-CH_{ar}); $^{31}P\{^1H\}$ (CD_2Cl_2): $\delta = 26$ (brs) (295 K); $C_{112}H_{126}P_6O_4Cl_2Co_2B_2F_8$ (2084.5): calcd. for **3**·1.5CH_2Cl_2: C 61.63, H 5.88; found C 61.79, H 6.15.

(μ-X-Anilato)bis[{1,1,1-tris(diphenylphosphanomethyl)ethane}cobalt]bis(hexafluorophosphate) (5a–b): A solution of $CoCl_2$ (130 mg, 1 mmol) in ethanol (15 mL) was added to a solution of the tripod ligand (624 mg, 1 mmol) in THF (15 mL). Addition of the coligand (X = H: 70 mg; X = Cl: 105 mg, 0.5 mmol) to the red solution caused an immediate change to dark green. After addition of solid $NaPF_6$ (168 mg, 1 mmol) in one portion and stirring for one hour the precipitated complex salt was filtered off, washed with diethyl ether (2 × 10 mL), cold ethanol (2 × 10 mL) and again diethyl ether (2 × 10 mL). The solid residue was taken up in methylene chloride and undissolved NaCl was filtered off. Recrystallisation from methylene chloride/diethyl ether yielded **5a** (405 mg, 45%) and **5b** (494 mg, 53%), respectively.

5a: M.p. 295 °C (decomp.); IR (CsI): $\tilde{\nu} = 3061\ cm^{-1}$ (m), 1584 (m), 1573 (m), 1483 (s), 1436 (s), 1255 (s), 1193 (s), 1094 (s), 998 (m), 857 (br), 740 (s), 696 (s); ^1H NMR (CD_2Cl_2): $\delta = 1.80$ (s, 3H, CH_3), 2.68 (brs, 6H, CH_2), 6.98 (s, 1H, ligand-CH), 7.2 (brs, 30H, CH_{ar}); $^{31}P\{^1H\}$ (CD_2Cl_2): $\delta = 29$ (brs, 2P, tripod-*P*), −144.2 (sept., $^1J_{PF} = 711$ Hz, 1P, PF_6) (195 K); $C_{88}H_{80}P_8O_4Co_2F_{12}$ (1795.2): calcd. for **5a**·1.0CH_2Cl_2: C 56.86, H 4.40, P 13.18; found C 56.45, H 4.55, P 13.07.

5b: M.p. 303 °C (decomp.); IR (CsI): $\tilde{\nu} = 3057\ cm^{-1}$ (m), 1584 (m), 1573 (m), 1484 (s), 1435 (s), 1385 (m), 1255 (s), 1193 (s), 1155 (s), 1094 (s), 998 (m), 857 (br), 740 (s), 696 (s); ^1H NMR ([D_6]acetone): $\delta = CH_3$ under solvent signal, 2.97 (brs, 6H, CH_2), 7.1–7.5 (m, 30H, CH_{ar}); $^{31}P\{^1H\}$ ([D_6]acetone): $\delta = 30$ (brs, 2P, tripod-*P*), −144.2 (sept., $^1J_{PF} = 711$ Hz, PF_6) (280 K): $\delta = 31$ (s, 3P, tripod-*P*), −144.2 (sept., $^1J_{PF} = 711$ Hz, PF_6) (270 K): $C_{88}H_{78}P_8O_4Cl_2Co_2F_{12}$ (1864.1): calcd. for **5b**·1.5CH_2Cl_2: C 53.98, H 4.10; found C 54.22, H 4.28.

(4,5-Methylenedioxycatecholato)[{1,1,1-tris(diphenylphosphanomethyl)ethane}cobalt](tetrafluoroborate) (6): To a solution of the tripod ligand (624 mg, 1 mmol) in THF (15 mL) a solution of $[Co(BF_4)_2]\cdot 6H_2O$ (341 mg, 1 mmol) in ethanol (15 mL) was added. Addition of 4,5-methylenedioxy-1,2-benzoquinone (152 mg, 1.0 mmol) to the orange-red coloured solution caused an immediate colour change to bright blue. After stirring the solution for one hour the solution was filtered. The reaction mixture was concentrated in vacuo until **6** started to precipitate. The complex salt was filtered off, washed with cold ethanol (10 mL) and twice with diethyl ether (10 mL portions). Recrystallisation from methylene chloride/diethyl ether yielded **6** (720 mg, 78%). Vapour diffusion of diethyl ether into a methylene chloride solution of the complex afforded dark blue crystals suitable for X-ray crystallographic analysis; M.p. 276 °C; IR (CsI): $\tilde{\nu} = 3055\ cm^{-1}$ (m), 1583 (m), 1498 (m), 1484 (m), 1460 (s), 1435 (s), 1340 (m), 1324 (s), 1273 (m), 1191 (s), 1094 (s), 1057 (br), 995 (m), 942 (m), 833 (m), 742 (m), 697 (s); UV/Vis/NIR (CH_2Cl_2): λ_{max} (ε, $M^{-1}cm^{-1}$) = 303 nm (17950), 412 nm (2320, sh), 673 nm (6980), 796 nm (13450); MS (FAB): *m/z* (%): 835 (100) [M^+], 683 (12) [tripodCo$^+$]; ^1H NMR (CD_2Cl_2): $\delta = 1.83$ (s, 3H, CH_3), 2.53 (brs, 6H, CH_2), 6.84 (s, 2H, ligand-CH), 7.0–7.2 (m, 32H, CH_{ar} + O-CH_2-O); $^{31}P\{^1H\}$ (CD_2Cl_2): $\delta = 35.6$ (s) (295 K); $^{13}C\{^1H\}$ NMR (CD_2Cl_2): 31.7 (m, tripod-CH_2), 36.5 (q, $^3J_{CP} = 11$ Hz, tripod-CH_3), 38.4 (s, tripod-C_q), 101.9, 104.7 (s, ligand-*CH*, ligand O-CH_2-O), 129.0, 130.8, 132.4 (m, tripod-CH_{ar}), 133.2 (m, tripod-C_{ipso}), 149.6 (s, ligand-*C*O-CH_2), 168.0 (s, ligand-*C*O-Co); $C_{48}H_{43}P_3O_4CoBF_4$ (922.5): calcd. for **6**·0.5CH_2Cl_2: C 60.37, H 4.60; found C 60.72, H 5.10.

(4,5-Methylenedioxycatecholato)[{1,1,1-tris(diphenylphosphanomethyl)ethane}cobalt](hexafluorophosphate) (7): A solution of $CoCl_2$ (130 mg, 1 mmol) in ethanol (15 mL) was added to a solution of the tripod ligand (624 mg, 1 mmol) in THF (15 mL). Addition of 4,5-methylenedioxy-1,2-benzoquinone (152 mg, 1.0 mmol) to the red solution caused an immediate change to bright blue. After addition of solid $NaPF_6$ (168 mg, 1 mmol) in one portion and stirring for one hour the precipitated complex salt was filtered off, washed with diethyl ether (2 × 10 mL), cold ethanol (2 × 10 mL) and again diethyl ether (2 × 10 mL). The solid residue was taken up in methylene chloride and undissolved NaCl was filtered off. Recrystallisation from methylene chloride/diethyl ether affords **7** (430 mg, 43%); M.p. 230 °C; IR (CsI): $\tilde{\nu} = 3059\ cm^{-1}$ (m), 1586 (m), 1462 (m), 1437 (m), 1339 (m), 1155 (m), 1094 (s), 1031 (m), 998 (m), 944 (m), 841 (br), 739 (m), 697 (s); UV/Vis/NIR (CH_2Cl_2): λ_{max} (ε, $M^{-1}cm^{-1}$) = 298 nm (16940), 414 (2180, sh), 671 (6070), 795 (11220); MS (FAB): *m/z* (%): 835 (100) [M^+], 683 (15) [tripodCo$^+$]; ^1H NMR (CD_2Cl_2): $\delta = 1.71$ (s, 3H, CH_3), 2.47 (brs, 6H, CH_2), 6.83 (s, 2H, ligand-CH), 7.0–7.2 (m, 32H, CH_{ar} + O-CH_2-O); $^{31}P\{^1H\}$ (CD_2Cl_2): $\delta = 35.6$ (s, 3P, tripod-*P*), −144.2 (sept., $^1J_{PF} = 713$ Hz, 1P, PF_6) (295 K); $C_{48}H_{43}P_4O_4CoF_6$ (980.7): calcd. for **6**·1.0CH_2Cl_2: C 55.23, H 4.26, P 11.63; found C 55.64, H 4.49, P 12.06.

X-ray structure determinations: The measurements were carried out on a Siemens P4 (Nicolet Syntex) R3m/v four-circle diffractometer with graphite-monochromated $Mo_{K\alpha}$ radiation. All calculations were performed with the SHELXT PLUS software package. Structures were solved by direct methods with the SHELXS86 program and refined with the SHELX93 program.[48] An absorption correction (Ψ scan, ΔΨ = 10°) was applied to all data. Atomic coordinates and anisotropic thermal parameters of the non-hydrogen atoms were refined by full-matrix least-squares calculation. Table 5 contains the

Table 5. Crystal data and structural analysis results for **1**, **2a**, **2b**, **2c** and **6**.

	1	**2a**·4CH_2Cl_2	**2b**·2$(CH_3)_2CO$	**2c**·1CH_3CN	**6**·0.5CH_2Cl_2
formula (without solvates)	$C_{84}H_{78}P_6Co_2O_4B_2F_8$	$C_{88}H_{80}P_6Co_2O_4B_2F_8$	$C_{88}H_{78}P_6Co_2O_4Cl_2B_2F_8$	$C_{88}H_{78}P_6Co_2O_4Br_2B_2F_8$	$C_{48}H_{43}P_3CoO_4BF_4$
M_r [g mol^{-1}] (without solvates)	1628.86	1678.92	1747.81	1836.71	922.53
crystal dimensions [mm] (without solvates)	0.50 × 0.30 × 0.30	0.30 × 0.30 × 0.20	0.20 × 0.20 × 0.30	0.20 × 0.20 × 0.20	0.30 × 0.30 × 0.30
crystal system	triclinic	monoclinic	triclinic	monoclinic	monoclinic
Z	1	2	1	2	4
space group (no.)	$P\bar{1}$ (2)	$P2_1/n$ (14)	$P\bar{1}$ (2)	$P2_1/c$ (14)	$P2_1/c$ (14)
a [pm]	1226.6(4)	1240.0(2)	1203.0(2)	1225.9(2)	1590.3(2)
b [pm]	1278.7(3)	1255.0(3)	1365.1(3)	1364.5(3)	1420.6(4)
c [pm]	1429.0(3)	3050.0(6)	1441.8(3)	2643.3(4)	2000.5(2)
α [°]	112.78(2)	90.00(0)	72.35(2)	90.00(0)	90.00(0)
β [°]	96.49(2)	101.54(3)	83.77(1)	94.39(1)	105.21(1)
γ [°]	98.64(2)	90.00(0)	89.00(1)	90.00(0)	90.00(0)
V [10^6 pm^3]	2006.7(9)	4651(2)	2196.0(8)	4409(1)	4361(1)
ρ_{calcd} [g cm^{-3}]	1.348	1.442	1.400	1.414	1.465
T [K]	295	210	150	200	200
no. rflns for cell parameter refinement	25	25	31	30	30
2θ range [°]	3.1–55.1	3.4–52.0	3.1–45.0	4.3–54.0	3.6–52.0
scan speed [° min^{-1}]	6.0 < ω < 29.3	6.0 < ω < 29.3	10.0	12.0	8.0 < ω < 60.0
no. rflns measured	9271	7352	6025	9919	8902
no. unique rlfns	9271	7150	5694	9477	8584
no. reflns observed	6766	4357	4448	4168	6413
obs. criterion	$I > 2\sigma(I)$	$I > 2\sigma(I)$	$I > 2\sigma(I)$	$I > 2\sigma(I)$	$I > 2\sigma(I)$
no. of LS parameters	526	633	545	515	587
R_1 [%]	6.8	6.9	5.1	9.8	5.2
R_w [%] (refinement on F^2)	14.6	17.2	14.3	30.1	13.9

0947-6539/97/0305-0742 $ 17.50+.50/0 Chem. Eur. J. 1997, 3, No. 5

data for the structure determinations. Further details of the crystal structure investigations may be obtained from the Fachinformationszentrum Karlsruhe, D-76344 Eggenstein-Leopoldshafen (Germany), on quoting the depository numbers CSD-406045 (**1**), CSD-406046 (**2a**), CSD-406043 (**2b**), CSD-406047 (**2c**) and CSD-406044 (**6**).

Acknowledgements: This work was supported by the Deutsche Forschungsgemeinschaft, the Fonds der Chemischen Industrie and the Volkswagenstiftung. We are particularly indebted to Prof. Dr. Karl Wieghardt for his continued interest and for his advice in practice as well as in theory.

Received: November 15, 1996 [F519]

[1] C. G. Pierpont, C. W. Lange, *Prog. Inorg. Chem.* **1993**, *41*, 381.
[2] R. M. Buchanan, C. Wilson-Blumenberg, C. Trapp, S. K. Larsen, D. L. Greene, C. G. Pierpont, *Inorg. Chem.* **1986**, *25*, 3070.
[3] G. A. Razuvaev, V. K. Cherkasov, G. A. Abakumov, *J. Organomet. Chem.* **1978**, *160*, 361.
[4] M. Haga, E. S. Dodsworth, A. B. P. Lever, *Inorg. Chem.* **1986**, *25*, 447.
[5] a) C. Bianchini, D. Masi, C. Mealli, A. Meli, G. Martini, F. Laschi, P. Zanello, *Inorg. Chem.* **1987**, *26*, 3683; b) S. Vogel, G. Huttner, L. Zsolnai, *Z. Naturforsch.* **1993**, *48b*, 641.
[6] a) A. B. P. Lever, P. R. Auburn, E. S. Dodsworth, M. Haga, W. Liu, M. Melnik, W. A. Nevin, *J. Am. Chem. Soc.* **1988**, *110*, 8076; b) S. R. Boone, C. G. Pierpont, *Polyhedron* **1990**, *9*, 2267.
[7] a) R. M. Buchanan, C. G. Pierpont, *J. Am. Chem. Soc.* **1980**, *102*, 4951; b) D. M. Adams, A. Dei, A. L. Rheingold, D. N. Hendrickson, *ibid.* **1993**, *115*, 8221; c) D. M. Adams, A. Dei, A. L. Rheingold, D. N. Hendrickson, *Angew. Chem.* **1993**, *105*, 954; *Angew. Chem. Int. Ed. Engl.* **1993**, *32*, 880; d) C. G. Pierpont, O.-S. Jung, *Inorg. Chem.* **1995**, *34*, 4281; e) O.-S. Jung, C. G. Pierpont, *ibid.* **1994**, *33*, 2227; f) O.-S. Jung, D. Hwan Jo, Y.-A. Lee, Y. Soo Sohn, C. G. Pierpont, *Angew. Chem.* **1996**, *108*, 1796; *Angew. Chem. Int. Ed. Engl.* **1996**, *35*, 1694; g) O.-S. Jung, C. G. Pierpont, *J. Am. Chem. Soc.* **1994**, *116*, 1127; h) C. Roux, D. M. Adams, J. P. Itié, A. Polian, D. N. Hendrickson, M. Verdaguer, *Inorg. Chem.* **1996**, *35*, 2846; i) O.-S. Jung, C. G. Pierpont, *J. Am. Chem. Soc.* **1994**, *116*, 2229; j) D. M. Adams, B. Li, J. D. Simon, D. N. Hendrickson, *Angew. Chem.* **1995**, *107*, 1580; *Angew. Chem. Int. Ed. Engl.* **1995**, *34*, 1481.
[8] a) M. W. Lynch, D. N. Hendrickson, B. J. Fitzgerald, C. G. Pierpont, *J. Am. Chem. Soc.* **1984**, *106*, 2041; b) A. S. Attia, C. G. Pierpont, *Inorg. Chem.* **1995**, *34*, 1172.
[9] a) J. V. Folgado, R. Ibáñez, E. Coronado, D. Beltrán, J. M. Savariault, J. Galy, *Inorg. Chem.* **1988**, *27*, 19; b) C. Fujii, M. Mitsumi, M. Kodera, K.-I. Motoda, M. Ohba, N. Matsumoto, H. Okawa, *Polyhedron* **1994**, *13*, 933; c) F. Tinti, M. Verdaguer, O. Kahn, J.-M. Savariault, *Inorg. Chem.* **1987**, *26*, 2380.
[10] C. G. Pierpont, L. C. Francesconi, D. N. Hendrickson, *Inorg. Chem.* **1977**, *16*, 2367.
[11] a) J. T. Wrobleski, D. B. Brown, *Inorg. Chem.* **1979**, *18*, 498; b) F. Lloret, M. Julve, J. Faus, X. Solans, Y. Journaux, I. Morgenstern-Badarau, *ibid.* **1990**, *29*, 2232.
[12] M. A. Calvo, A. M. Manotti Lanfredi, L. A. Oro, M. T. Pinillos, C. Tejel, A. Tirpicchio, F. Ugozzoli, *Inorg. Chem.* **1993**, *32*, 1147.
[13] M. D. Ward, *Inorg. Chem.* **1996**, *35*, 1712.
[14] a) L. Sacconi, S. Midollini, *J. Chem. Soc. Dalton Trans.* **1972**, 1213; b) C. Mealli, S. Midollini, L. Sacconi, *Inorg. Chem.* **1975**, *14*, 2513; c) V. Sernau, G. Huttner, J. Scherer, O. Walter, *Chem. Ber.* **1996**, *129*, 243; d) V. Sernau, G. Huttner, J. Scherer, L. Zsolnai, T. Seitz, *ibid.* **1995**, *128*, 193.
[15] V. Körner, A. Asam, G. Huttner, L. Zsolnai, *Z. Naturforsch.* **1994**, *49b*, 1183.
[16] a) M. Di Vaira, M. Perruzzini, P. Stoppioni, *J. Chem. Soc. Dalton Trans.* **1984**, 359; b) C. Bianchini, A. Meli, A. Orlandini, *Inorg. Chem.* **1982**, *21*, 4161; c) C. A. Ghilardi, S. Midollini, L. Sacconi, *ibid.* **1977**, *16*, 2377; d) S. Vogel, A. Barth, G. Huttner, T. Klein, L. Zsolnai, R. Kremer, *Angew. Chem.* **1991**, *103*, 325; *Angew. Chem. Int. Ed. Engl.* **1991**, *30*, 303; e) S. Vogel, G. Huttner, L. Zsolnai, C. Emmerich, *Z. Naturforsch.* **1993**, *48b*, 353.
[17] a) J. Glerup, P. A. Goodson, D. J. Hodgson, K. Michelsen, *Inorg. Chem.* **1995**, *34*, 6255; b) T. R. Felthouse, E. J. Laskowski, D. N. Hendrickson, *ibid.* **1977**, *16*, 1077; c) D. M. Duggan, D. N. Hendrickson, *ibid.* **1973**, *12*, 2422; d) M. Julve, M. Verdaguer, O. Kahn, *ibid.* **1983**, *22*, 368; e) M. Julve, M. Verdaguer, A. Gleizes, M. Philoche-Levisalles, O. Kahn, *ibid.* **1984**, *23*, 3808.
[18] O. Kahn, *Molecular Magnetism*, VCH, Weinheim (Germany), **1993**.
[19] C. A. Ghilardi, C. Mealli, S. Midollini, V. I. Nefedov, A. Orlandini, L. Sacconi, *Inorg. Chem.* **1980**, *19*, 2454.
[20] K. Heinze, S. Mann, G. Huttner, L. Zsolnai, *Chem. Ber.* **1996**, *129*, 1115.
[21] E. Krogh Anderson, *Acta Crystallogr.* **1967**, *22*, 196.
[22] E. Krogh Anderson, *Acta Crystallogr.* **1967**, *22*, 201.
[23] A. Barth, G. Huttner, M. Fritz, L. Zsolnai, *Angew. Chem.* **1990**, *102*, 956; *Angew. Chem. Int. Ed. Engl.* **1990**, *29*, 929.
[24] S. Aime, R. Gobetto, D. Osella, L. Milone, G. E. Hawkes, E. W. Randall, *J. Magn. Reson.* **1985**, *65*, 308.
[25] T. Beringhelli, G. D. Alfonso, M. Freni, A. P. Minoja, *Inorg. Chem.* **1996**, *35*, 2393.
[26] As the phosphorus nuclei of the PF_6^- anion have a significantly lower relaxation rate than the phosphorus nuclei bound to cobalt ion the relaxation delay between two pulses has to be increased. The necessary delay time was determined experimentally by measuring the $^{31}P\{^1H\}$ NMR spectra of compound **7** $[(tripod)Co(C_7H_4O_4)]^+ PF_6^-$ with different delay times (0.1 to 3 s). With a relaxation delay time of about 2 s the intensities of the $P(PF_6)$ and P(tripod) signals have reached their theoretical ratio of 1:3, which does not change with further increase in the relaxation delay time. The $^{31}P\{^1H\}$ NMR spectra of the dinuclear complexes **5a** and **5b** were therefore measured with a relaxation delay time of 2.5 s (in the range $\delta = +70$ to -190, 512 scans).
[27] a) M. B. Robin, P. Day, *Adv. Inorg. Chem. Radiochem.* **1967**, *10*, 247; b) C. Creutz, *Prog. Inorg. Chem.* **1983**, **30**, 1.
[28] The complex $[(tripod)Co(cat)]^+[BPh_4^-]$ was prepared according to the literature (ref. [5b]). A 10^{-3} M solution of this compound in THF/CH_2Cl_2 (2:1) was cooled to 100 K and the electronic spectra were measured.
[29] Acetonitrile (1167 nm), methanol (1171 nm), ethanol (1175 nm), acetone (1183 nm), ethyl acetate (1183 nm), methylene chloride (1185 nm), nitromethane (1186 nm), chloroform (1188 nm), tetrahydrofuran (1191 nm), isopropanol (1197 nm), dioxane (1215 nm), benzene (1279 nm).
[30] The calculations were performed on an Apple Macintosh IIfx with the CAChe/ZINDO program Version 3.6 (M. C. Zerner, **1990 1994**) with INDO/1 parameters. As the molecules were found to be closed-shell a spin-restricted calculation (RHF) was applied. The geometry of the molecules was taken from the X-ray structural analyses. The tripod ligand was replaced by three isoelectronic PH_3 groups. C_i molecular symmetry was maintained for the dinuclear model complex and the mononuclear model complex was idealised to C_s symmetry.
[31] a) M. C. Zerner, *Reviews in Computational Chemistry*, VCH, Weinheim (Germany), **1991**, p. 313; b) J. A. Pople, *J. Chem. Phys.* **1967**, *47*, 2026; c) M. Kotzian, N. Rösch, H. Schröder, M. C. Zerner, *J. Am. Chem. Soc.* **1989**, *111*, 7687; d) J. Ridley, M. C. Zerner, *Theoret. Chim. Acta (Berlin)* **1973**, *32*, 111.
[32] a) A. R. Rossi, R. Hoffmann, *Inorg. Chem.* **1975**, *14*, 365; b) M. Elian, M. M. L. Chen, D. M. P. Mingos, R. Hoffmann, *ibid.* **1976**, *15*, 1148; c) T. A. Albright, *Tetrahedron*, **1982**, *38*, 1339.
[33] Configuration interaction HOMO − 13, LUMO + 13, single excitations, singlets; calculated energy for the HOMO → LUMO transition 15440 cm^{-1} (CI coefficient $c^2 = 0.52$, next largest coefficient $c^2 = 0.15$, oscillator strength 0.87); calculated energy for the (HOMO − 1) → LUMO transition 20400 cm^{-1} (CI coefficient $c^2 = 0.80$, next largest coefficient $c^2 = 0.07$, oscillator strength 0.03); the energy is calculated too high by a factor of approximately 1.8; the intensity is overestimated by a factor of 2 (refs. [31c,d]).
[34] E. Krogh Anderson, *Acta Crystallogr.* **1967**, *22*, 204.
[35] A. Streitwieser, C. H. Heathcock, *Introduction to Organic Chemistry*, 3rd ed., Macmillan, New York, **1985**; *Organische Chemie*, VCH, Weinheim (Germany), **1986**.
[36] a) M. D. Ward, *Chem. Soc. Rev.* **1995**, *24*, 121 and references cited therein; b) G. S. Hanan, C. R. Arana, J.-M. Lehn, G. Baum, D. Fenske, *Chem. Eur. J.* **1996**, *2*, 1292; c) G. Giuffrida, S. Campagna, *Coord. Chem. Rev.* **1994**, *135/136*, 517.
[37] Configuration interaction HOMO − 13, LUMO + 13, single excitations, singlets; calculated energy for the HOMO → LUMO transition 17700 cm^{-1} (CI coefficient $c^2 = 0.74$, next largest coefficient $c^2 = 0.09$, oscillator strength 0.37); calculated energy for the (HOMO − 1) → LUMO transition 23530 cm^{-1} (CI coefficient $c^2 = 0.90$, next largest coefficient $c^2 = 0.06$, oscillator strength 0.06); the energies are calculated too high by a factor of approximately 1.2; the intensities are overestimated by a factor of 5 (refs. [31c,d]).
[38] a) D. F. Evans, *J. Chem. Soc.* **1959**, 2003; b) T. H. Crawford, J. Swanson, *J. Chem. Educ.* **1971**, *48*, 382.
[39] a) W. Hewertson, H. R. Watson, *J. Chem. Soc.* **1962**, 1490; b) A. Muth, Diplomarbeit, University of Heidelberg, **1989**.
[40] A. Muth, O. Walter, G. Huttner, A. Asam, L. Zsolnai, C. Emmerich, *J. Organomet. Chem.* **1994**, *468*, 149.
[41] A. V. El'tsov, *J. Org. Chem. USSR*, **1963**, *33*, 1952.
[42] W. Flaig, T. Ploetz, H. Biergans, *Liebigs Ann. Chem.* **1955**, *597*, 196.
[43] H. A. Torrey, W. H. Hunter, *J. Am. Chem. Soc.* **1912**, 34, 702.
[44] H. O. Meyer, *Ber. Dtsch. Chem. Ges.* **1924**, *57*, 326.
[45] F. Kögl, A. Lang, *Ber. Dtsch. Chem. Ges.* **1926**, *59*, 910.
[46] F. Fichter, A. Willmann, *Ber. Dtsch. Chem. Ges.* **1904**, 37, 2384.
[47] F. Fichter, *Liebigs Ann. Chem.* **1908**, 361, 363.
[48] a) G. M. Sheldrick, *SHELXS 86, Program for Crystal Structure Solution*, University of Göttingen, **1986**; b) G. M. Sheldrick, *SHELXL 93, Program for Crystal Structure Refinement*, University of Göttingen, **1993**.
[49] Here a numbering scheme identical for all complexes is used for the sake of easier comparison, unlike the numbering schemes of the deposited structures.